Surface-Stabilized Amorphous Germanium Nanoparticles for Lithium-Storage Material

Hyojin Lee,[†] Min Gyu Kim,[‡] Cheol Ho Choi,[§] Yang-Kook Sun,[||] Chong Seung Yoon,[⊥] and Jaephil Cho*[,†]

Department of Applied Chemistry, Kumoh National Institute of Technology, Gumi, Korea, Beamline Research Division, Pohang Accelerator Laboratory, Pohang University of Science and Technology, Pohang, Korea, Department of Chemistry, Kyungpook National University, Taegu, Korea, Department of Chemical Engineering, and Division of Materials Science and Engineering, Hanyang University, Seoul, Korea

Received: May 18, 2005; In Final Form: September 12, 2005

Amorphous Ge nanoparticles with the particle size of ∼10 nm were prepared by capping butyl groups and were characterized using XAS, TEM, FT-IR reflectance, and electrochemical cycling. The XAS results for the first-cycle Ge nanoparticles exhibited either a little particle aggregation after reformation of the Ge−Ge metallic bond or reformation of Ge−Ge metallic bond followed by a little particle aggregation. More interestingly, butyl groups, being electrochemically stable, remained after cycling, and the quantum mechanical calculation of the thermodynamic energy of the reaction using the GAMESS (General Atomic and Molecular Electronic Structure System) program suggested the formation of a very stable surface Ge−C bond that cannot be easily subjected to the subsequent chemical reactions. Initial charge capacity is 1470 mAh/g with an irreversible capacity ratio of 12%; no capacity fading was observed out to 30 cycles. Even at 5 C rate discharging, capacity retention was 98%, compared to that at 0.2 C rate discharging. In addition, the capacity was fully recovered at 0.2 C rate cycling.

Introduction

Recently, because of the capacity limit of the graphite in a Li-ion cell, studies on lithium reactive metals as alternative anodes have been investigated actively. Among these, Si, Ge, and Sn are the most popular and interesting materials. Si and Ge showed specific capacity of 4000 mAh/g and 1600 mAh/g, respectively, when forming the $Li_{21}M_5$ alloy.[1−4] Despite this capacity merit, these materials exhibited rapid capacity loss accompanied by a huge irreversible capacity; the bulk Si capacity approaches ∼0 mAh/g after several cycles. This is the result of pulverization of the Si particles, which electrically isolates the particles from the current collector.[5−7] Several methods have been investigated to overcome this problem. One method is to form a metal and graphite composite by ball milling. Here, the graphite either acts as a buffer zone or sustains electrical contact with the current collector during the lithium reaction.[8,9] For instance, a silicon and carbon composite showed a maximum reversible capacity of 1700 mAh/g but exhibited capacity fading. On the other hand, with a mechanically milled Si and graphite composite, the graphite particles were slowly separated from the Si resulting in rapid capacity fading. Another method, forming a thin film Si, showed reversible capacity of ∼2500 mAh/g. Here, capacity retention strongly depends on film thickness, and rapid capacity fading was observed when the thickness was over 250 nm.[10−12] On the other hand, it has been suggested that capacity loss occurs for a different reason in amorphous alloys. Beaulieu et al. have shown that in amorphous alloys of Si and Sn, the expansion upon lithium insertion is homogeneous and that 10−30 mm pieces of thin films expand and contract reversibly without further pulverization.[13] It appears that in these amorphous films, capacity loss occurs because electrical contact is lost to expanding and contracting particles undergoing large volume changes and not because of the pulverization that occurs in crystalline films. However, it is doubtful whether such high-cost sputtered thin films could be used in anodes of high-energy low-cost Li-ion batteries. In this regard, nanoscale anode metals with both particle size of ∼10 nm and an amorphous phase could be the best candidate for use in Li-ion batteries. In this paper, we report the synthesis and electrochemical properties of surface stabilized amorphous germanium nanoparticles using butyl. Advantages of this method are not only minimization of volume change of the particle but also minimization of the electrolyte decomposition on the anode surface that was a detrimental factor for increasing irreversible capacity.

Experimental Section

Sodium naphthalide solution was prepared from 0.69 g sodium and 2.93 g of naphthalene stirred in 70 cm^3 of 1.2-dimethoxyethane. $GeCl_4$ (1.04 g) and 1,2-dimethoxyethane (100 mL) were thoroughly mixed, and the mixture was poured into a sodium naphthalide solution. This mixed solution was stirred for 2 h, and then 0.1 g of butyllithium was added. Instantly, a yellow solution was obtained, and the solvent and naphthalene were removed using rotating evaporator. Finally, the resulting orange solution was washed with water six times and was dispersed in *n*-hexane, followed by vacuum-drying at 200 °C for 24 h. The final product was a solid form with a little viscosity.

The cathodes for the battery test cells were made of butyl-capped Ge material, Super P carbon black, and polyvinylidene

* Corresponding author. E-mail: jpcho@kumoh.ac.kr.
[†] Department of Applied Chemistry, Kumoh National Institute of Technology.
[‡] Beamline Research Division, Pohang Accelerator Laboratory, Pohang University of Science and Technology.
[§] Department of Chemistry, Kyungpook National University.
[||] Department of Chemical Engineering, Hanyang University.
[⊥] Division of Materials Science and Engineering, Hanyang University.

10.1021/jp052620y CCC: $30.25
Published on Web 10/13/2005

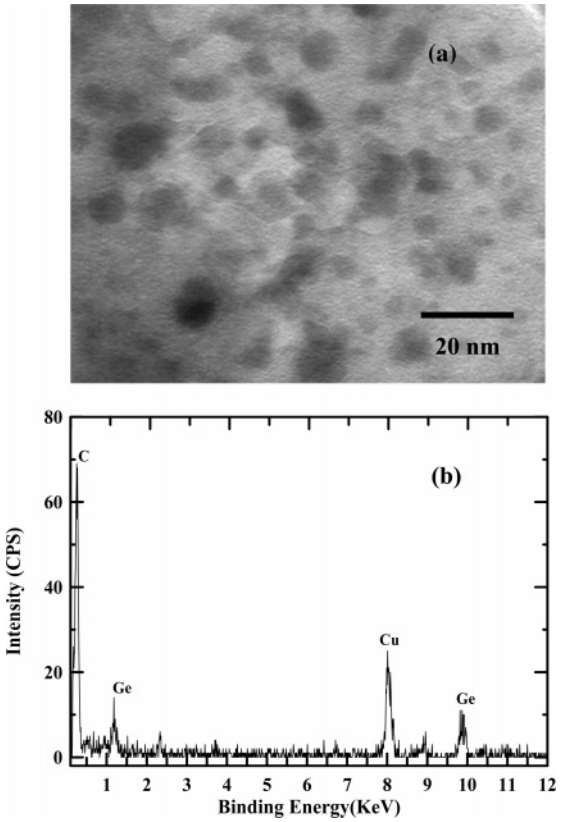

Figure 1. (a) TEM image of butyl-capped Ge nanoparticles and (b) EDX spectroscopy of the butyl-capped Ge nanoparticles. The Cu peak is from Cu grid.

fluoride (PVDF) binder in a weight ratio of 80:10:10. The slurry was prepared by thoroughly mixing an *N*-methyl-2-pyrrolidone (NMP) solution of PVDF (below 0.01% water), carbon black, and the anode material. The coin-type half cells (2016 size) prepared in a helium-filled glovebox contained a cathode, a Li metal anode, a microporous polyethylene separator, and an electrolyte solution of 1 M $LiPF_6$ in ethylene carbonate/dimethyl carbonate (EC/DMC) (1:1 vol. %).

Ge K-edge X-ray absorption spectra (XAS) of butyl-capped Ge nanoparticles for the first discharge−charge process were taken on a BL7C1 (Electrochemistry) beamline in a storage ring of 2.5 GeV with a ring current of 120−170 mA at the Pohang Light Source (PLS). A Si(111) double-crystal monochromator was employed to monochromatize the X-ray photon energy. Higher-order harmonic contaminations were eliminated by detuning the monochromator to reduce the incident X-ray intensity by ∼30%. The incident X-ray intensity was monitored with pure nitrogen gas-filled ionization chambers. The spectroscopic data were collected in transmittance mode. Energy calibration was made using standard metallic Ge foil.

Results and Discussion

Figure 1 shows a TEM image of the butyl-capped Ge nanoparticles with an average particle size of 10 nm. The different contrast in the particle indicates possible presence of the butyl-group on the particle surface. Energy dispersive spectroscopy of the particle in Figure 1a shows the Ge peaks at ∼1.1 and 9.9 keV, and no oxygen peak was detected at ∼350 eV. Figure 2 exhibits the X-ray diffraction pattern of the sample, showing the formation of the amorphous Ge phase. The formation of amorphous Ge nanoparticles was also reported by Taylor, where metathesis reactions between KGe and $GeCl_4$ in

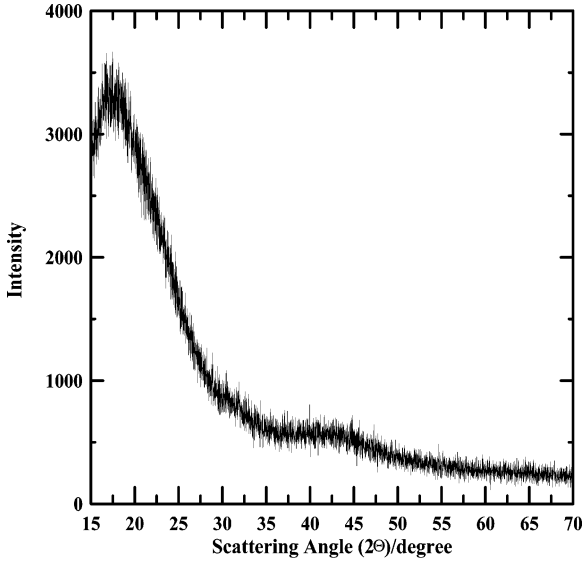

Figure 2. XRD pattern of butyl-capped Ge nanoparticles.

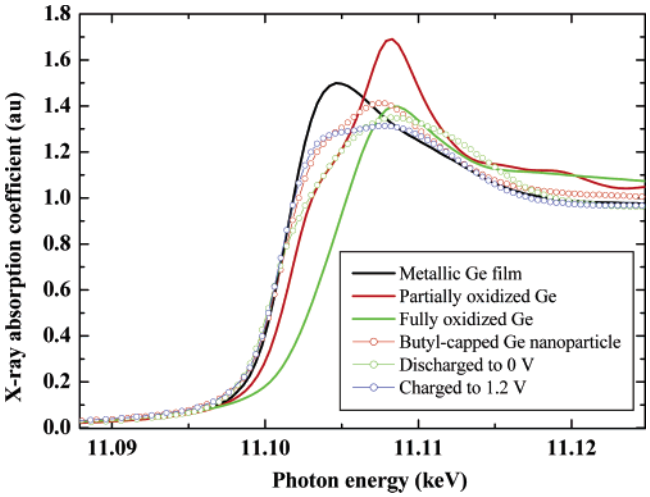

Figure 3. Normalized Ge K-edge XANES spectra for the butyl-capped Ge nanoparticle, metallic Ge tin film, and fully and partially oxidized Ge nanoparticles, in addition to those of the first-discharged and charged Ge nanoparticles.

ethylene glycol dimethyl ether (glyme) led to an amorphous phase.[14] On the other hand, the reduction of $GeCl_4$ and $RGeCl_3$ by Na dispersion in heptane and the reduction of the $GeCl_4$ by Li naphthalide showed the crystalline Ge.[15−19] Turner et al. reported that use of amorphous materials for the elimination of two-phase regions between phases of different lithium concentrations leads to homogeneous volume expansions and results in improved cycle life.[20] Moreover, butyl groups capped on Ge nanoparticles are expected to decrease the electrolyte decomposition reaction on the particle surface, thus decreasing the irreversible capacity. With respect to these results, the presence of amorphous Ge nanoparticles is expected to significantly improve capacity retention during lithium alloying/dealloying.

Figure 3 shows normalized Ge K-edge XANES spectra for the butyl-capped Ge nanoparticles, metallic Ge thin films, and fully and partially oxidized Ge nanoparticles, in addition to those of the first discharged and charged Ge nanoparticles. For the butyl-capped nanoparticle, the white line at ∼11.105 keV corresponds to the electric dipole-allowed transition of the 1s electron to an unoccupied 4p orbital. The peak position of the pristine is consistent with that of reference metallic Ge film, which directly shows that the as-prepared butyl-capped Ge

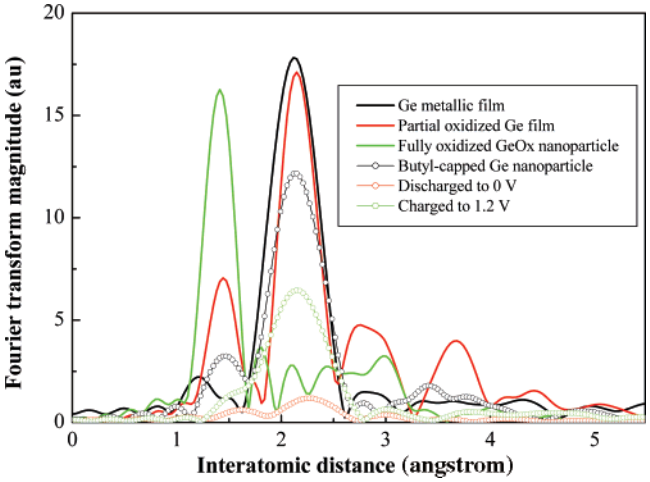

Figure 4. Fourier transform (FT) magnitudes of the Ge K-edge k^3-weighted EXAFS spectra for the butyl-capped Ge metallic nanoparticles, in addition to those of Ge reference materials.

nanoparticle consists of a metallic phase. Since the electronic configuration of the Ge metallic phase is $[Ar]3d^{10}4s^24p^2$, the peak intensity of the white line is related to the concentration of the 4p hole state. Compared with the peak feature of the bulk metallic phase, the decrease of peak intensity is dominant in the pristine, indicating the decrease of the 4p hole concentration. The peak feature variation can be explained with the small particle size of the pristine Ge. As the particle size decreases, the surface distortion increases under the larger surface-to-volume ratio. Therefore, 3d−4p rehybridization by the lattice distortion results from partial distribution of 3d electrons into 4p orbitals (the decrease of the 4p hole concentration). As a result, the peak feature of the white line for butyl-capped Ge nanoparticles is the result of the decrease of p character in the 4p level. The first discharge to 0 V leads to a decrease in the peak intensity of the white line, and the consecutive charge to 1.2 V returns it to original peak intensity. It clearly shows that the electrochemical behavior of butyl-capped Ge nanoparticles for Li is reversible during the first cycle.

Figure 4 shows the Fourier transform (FT) magnitudes of the Ge K-edge k^3-weighted EXAFS spectra for butyl-capped Ge nanoparticles, in addition to those of the reference materials. Since EXAFS refinement is very sensitive to atomic local sites and does not depend on the long-range order of atomic arrangement, it is a powerful technique for local structural analysis. For the metallic film, a characteristic peak at ∼2.2 Å corresponds to metallic Ge−Ge bonds. On the other hand, partially oxidized Ge metallic film and fully oxidized GeOx nanoparticles show a strong peak evolution at ∼1.5 Å, which corresponds to the Ge−O bond. Even though butyl-capped Ge also shows peaks at ∼1.5 Å, these are believed to be from Ge−C interactions, confirming no GeOx formation. The FT peak intensity of Ge−Ge bonding for the pristine butyl-capped Ge nanoparticle, showing small FT peak intensity with respect to that of metallic Ge film, presents a nanosized Ge metallic particle. The fact can be supported with TEM results. In fully discharged Ge nanoparticles, the FT peak decreases abruptly, meaning Ge−Ge metallic-bond cleavage or formation of Ge or Ge−C clusters. The consecutive charge to 1.2 V leads to abrupt increase of FT peak intensity. This is the result of a little particle aggregation after reformation of the Ge−Ge metallic bonding from the Ge cluster. However, the peak intensity is about half that of the pristine butyl-capped Ge nanoparticles, which shows a noticeable decrease in particle size after the first cycle. Finally, it is expected that the lithiation of the butyl-capped nanoparticle

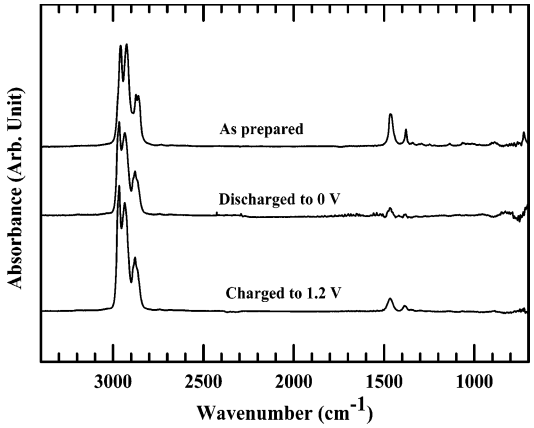

Figure 5. FT-IR reflectance spectra of the as-prepared butyl-capped Ge nanoparticles, discharged Ge nanoparticles to 0 V, and those charged to 1.2 V.

results in a Ge cluster-like particle through the incorporation of a Li atom into Ge−Ge bond. In the following delithiation, the Ge cluster is rearranged and aggregated to be smaller than that of pristine butyl-capped Ge nanoparticle.

FT-IR reflectance spectroscopy was used to identify and characterize organic species on the Ge nanoparticle surface. Figure 5 shows FT-IR reflectance spectroscopy of the as-prepared Ge nanoparticles terminated with *n*-butyl. Three characteristic bands are observed: 2970−2820, 1460−1360, and 900−800 cm^{-1}. The first band (2970−2820 cm^{-1}) is assigned to the Ge−CH_3 or C−CH_2 vibration mode, and the second band at 1460−1360 cm^{-1} is assigned to the C−CH_3 vibration mode. It has been reported that the Ge−C stretch for alkyl-capped Ge is typically seen at ∼860 cm.[14] The Ge−O stretch is typically observed at 870−910 cm^{-1} and is broad (some overlap of the Ge−C and Ge−O peaks is expected). Hence, the broad band between 800 and 900 cm^{-1} is a mixture of these peaks, indicating the presence of either a very small amount of oxygen on the surface or a very small amount of Ge−O-containing impurity in the sample. At the least, the butyl termination is believed to prevent the oxidation of the particles and provides a stable passivation layer. Furthermore, we found that Ge−C bonds are quite stable in the colloids, which were heated to 130 °C for 3 days without producing sufficient oxide to detect by FT-IR.

Figure 5 exhibits FT-IR spectra of the discharged and charged electrode, 0 V and 1.2 V, respectively. Even though we expected the *n*-butyl group capped on the particle surface to be decomposed during Li alloying/dealloying, the characteristic vibrational bands at 2970−2820 cm^{-1} were apparently shown during cycling, indicating that the C_4H_9 group was strongly bonded with Ge or Li_xGe_y alloys. To study the chemisorption thermodynamics of the lithium butane on a chlorinated Ge(111) surface, we adopted density functional theory (DFT) using the B3LYP[21] exchange-correlation functional in combination with the 6-31G(d)[22] basis set. The GAMESS[23] program was used for the computations. The $Ge_{26}H_{29}Cl$ cluster was designed to model the H-terminated Ge(111) surface. (As shown in Figure 6, one surface H atom was replaced with a Cl atom to model the chlorinated Ge surface.) The thermodynamic energy of the reaction described in Figure 6 was calculated to be −47.1 kcal/mol, indicating the formation of a very stable surface Ge−C bond that cannot be easily subjected to subsequent chemical reactions.

Figure 7a shows the voltage profiles of the butyl-capped amorphous Ge nanoparticles in a coin-type half cell between 0

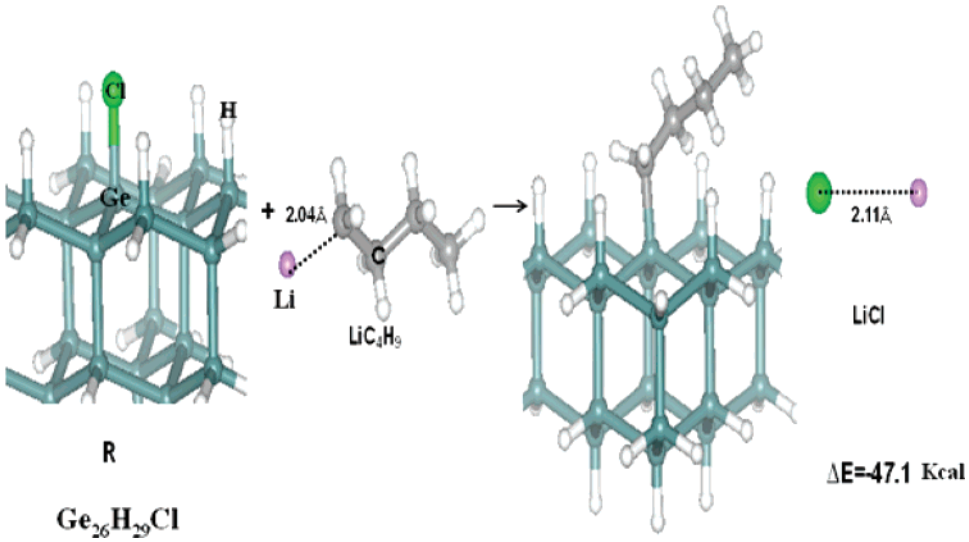

Figure 6. The reactants and products of LiC_4H_9 chemisorption on chlorinated Ge(111) surface.

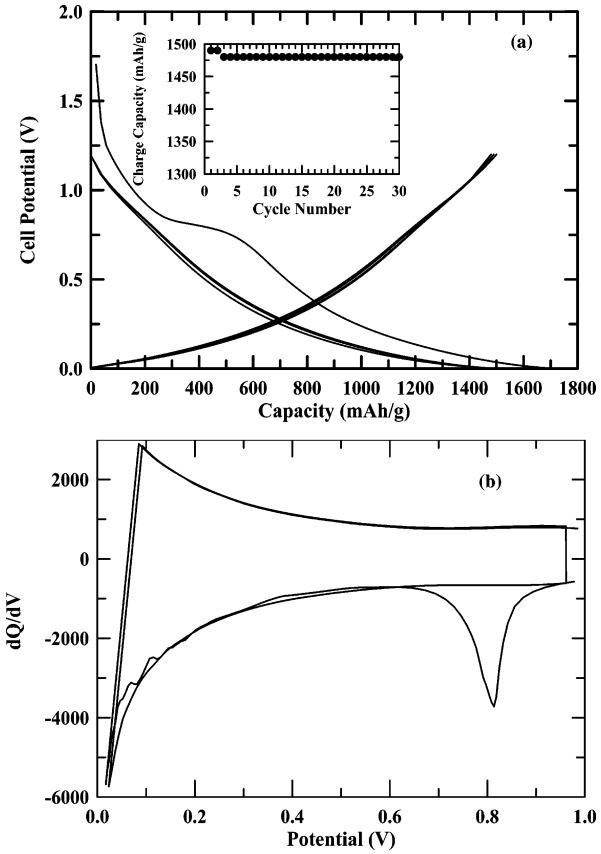

Figure 7. (a) Voltage profiles of the butyl-capped Ge nanoparticle anode in a coin-type half cell after 1, 5, 10, 20, and 30 cycles at a rate of 0.2 C (1 C = 1500 mA/g) between 0 and 12. V. The inset is the cycle number vs charge capacity of the butyl-capped Ge nanoparticle anode in a coin-type half cell. (b) Differential charging and discharging voltage profiles of the butyl-capped Ge anode for the first and second discharge and charge of the cell.

and 1.2 V at the rate of 0.2 C (1 C = 1500 mA/g) after 1, 5, 10, 20, and 30 cycles. Initial charge capacity is 1470 mAh/g with an irreversible capacity of 12%. Even after 30 cycles, there is no capacity decay. Using nanoparticles is far more superior to the method reported by Graetz et al. (size was not reported) which showed specific capacity of 1200 mAh/g, decreasing to 900 mAh/g after 30 cycles at a rate of 1/30 C (1 C = 1500 mA/g) (capacity retention after 30 cycles was 75%).[1] Furthermore, our capacity retention is quite similar to that of the 50 nm thickness thin Ge film. Note that voltage versus capacity is smooth and continuous, showing the absence of any plateaus indicative of phase changes between 0.6 and 0 V during the reaction with Li (Figure 7b). The differential capacity shown in Figure 5b is smooth and free of sharp peaks. This result is similar to that observed in amorphous Si−Sn alloy.[24] It should be noted that the nature of the lithium-insertion reaction and the Li metal-alloy phases formed depend strongly on particle size, with smaller particle sizes showing improved capacity retention. However, this showed a very large irreversible capacity from the electrolyte decomposition on the particle surface.[25] This is the result of the formation of a surface-electrolyte interphase (SEI). A reaction of lithium with the electrolyte on the particle surface accompanies the initial lithiation of the metal electrode, forming a passivation layer. For instance, nanoparticle SnO_2-anode material showed extremely high irreversible capacity, over 150% of the reversible capacity.[25] In addition, we need to consider the loss of electrical contact of the particles as a result of the large volume change on cycling. This loss continuously generates new active surfaces that were previously passivated by the stable surface films. Hence, the repeated reaction between the electrolyte and metal induces capacity fading. However, our results indicate that these reactions likely did not occur in the butyl-capped Ge nanoparticles.

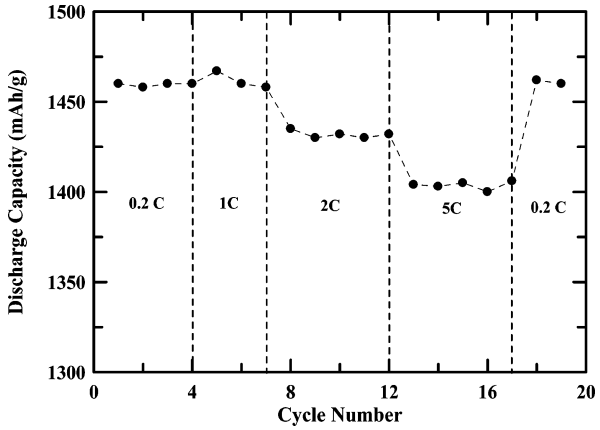

Figure 8. Rate capabilities of the butyl-capped Ge nanoparticle anode in a coin-type half cell at rates of 0.2, 0.5, 1, 2, and 5 C.

Finally, rate capability of the amorphous Ge nanoparticles in a coin-type half cell (anode was lithium metal) was tested at various C rates, as shown in Figure 8. The charging was fixed at a rate of 0.2 C, and the discharge rate was varied (0.2, 1, 2, and 5 C) with a different cycle number. Even at the 5 C discharging rate, the capacity retention was 98%, compared to that at the 0.2 C discharging rate. In addition, the capacity was fully recovered at the 0.2 C cycling rate.

Conclusions

Butyl-capped amorphous Ge nanoparticles exhibited excellent lithium-storage behavior during Li alloying and dealloying. The capping ligand played an important role in controlling the irreversible capacity, as opposed to lithium-storage metals which showed a large irreversible capacity. The initial capacity was 1470 mAh/g, and the capacity retention was 98% after 30 cycles. Furthermore, the sample had excellent rate capabilities, showing only a 2% capacity loss even at a 5 C cycling rate.

Acknowledgment. We are grateful to the authorities associated with Pohang Light Source (PLS) for XAS measurements. The experiments at PLS were supported in part by Korea MOST and POSTECH. This work was supported by University IT Research Center Project and by the Basic Research Program (R01-2004-000-10173-0) of KOSEF.

References and Notes

(1) Graetz, J.; Ahn, C. C.; Yazami, R.; Fultz, B. *J. Electrochem. Soc.* **2004**, *151*, A698.
(2) Obrovac, M. N.; Christensen, L. *Electrochem. Solid State Lett.* **2004**, *7*, A93.
(3) Weydanz, W. J.; Wohlfahrt-Mehrens, M.; Huggins, R. A. *J. Power Sources* **2003**, *81*, 237.
(4) Gao, B.; Sinha, S.; Fleming, L.; Zhou, O. *Adv. Mater.* **2001**, *13*, 816.
(5) Winter, M.; Bsenhard, J. O. *Electrochim. Acta* **2000**, *45*, 31.
(6) Boukamp, B. A.; Lesh, G. C.; Huggins, R. A. *J. Electrochem. Soc.* **1981**, *128*, 725.
(7) Wachtler, M.; Besenhard, J. O.; Winter, M. *J. Power Sources* **2001**, *94*, 189.
(8) Wang, G. X.; Yao, J.; Liu, H. K. *Electrochem. Solid State Lett.* **2004**, *7*, A250.
(9) Yang, J.; Wang, B. F.; Wang, K.; Liu, Y.; Xie, J. Y.; Wen, Z. S. *Electrochem. Solid State Lett.* **2003**, *6*, A154.
(10) Maranchi, J. P.; Hepp, A. F.; Kumta, P. N. *Electrochem. Solid State Lett.* **2003**, *6*, A198.
(11) Song, S.-W.; Striebel, K. A.; Reade, R. P.; Roberts, G. A.; Clairns, E. J. *J. Electrochem. Soc.* **2003**, 150, A121.
(12) Greatz, J.; Ahn, C. C.; Yazami, R.; Fultz, B. *Electrochem. Solid State Lett.* **2003**, *6*, A194.
(13) Beaulieu, L. Y.; Hatchard, T. D.; Bonakdarpour, A.; Fleischauer, M. D.; Dahn, J. R. *J. Electrochem. Soc.* **2003**, *150*, A1457.
(14) Taylor, B. R.; Kauzlarich, S. M. *Chem. Mater.* **1998**, *10*, 22.
(15) Taylor, B. R.; Kauzlarich, S. M. *Chem. Mater.* **1999**, *11*, 2493.
(16) Heath, J. R.; LeCoues, F. K. *Chem. Phys. Lett.* **1993**, *208*, 263.
(17) Heath, J. R.; Shiang, J. J.; Alivisatos, A. P. *J. Chem. Phys.* **1994**, *101*, 1607.
(18) Kornwski, A.; Giersig, M.; Vogel, R.; Chemseddine, A.; Weller, H. *Adv. Mater.* **1993**, *5*, 634.
(19) Wilcoxon, J. P.; Provencio, P. P.; Samara, G. A. *Phys. Rev. B* **2001**, *64*, 035417.
(20) Turner, R. L. World Intellectual Property Organization Patent Application WO 00/03444, 2000.
(21) (a) Becke, A. D. *J. Chem. Phys.* **1993**, *98*, 5648. (b) Stephens, P. J.; Devlin, F. J.; Chablowski, C. F.; Frisch, M. J. *J. Phys.Chem.* **1994**, *98*, 11623. (c) Hertwig, R. H.; Koch, W. *Chem. Phys. Lett.* **1997**, *268*, 345.
(22) Hehre, W. J.; Ditchfield, R.; Pople, J. A. *J. Chem. Phys.* **1972**, *56*, 2257.
(23) (a) Schmidt, M. W.; Baldridge, K. K.; Boatz, J. A.; Elbert, S. T.; Gordon, M. S.; Jensen, J. H.; Koseki, S.; Matsunaga, N.; Nguyen, K. A.; Su, S.; Windus, T. L.; Dupuis, M.; Montgomery, J. A., Jr. *J. Comput. Chem.* **1993**, *14*, 1347 (b) Fletcher, G. D.; Schmidt, M. W.; Gordon, M. S. *Adv. Chem. Phys.* **1999**, *110*, 267.
(24) Beaulieu, L. Y.; Hewitt, K. C.; Turner, R. L.; Bonadarpour, A.; Abdo, A. A.; Christensen, L.; Eberman, K. W.; Krause, L. J.; Dahn, J. R. *J. Electrochem. Soc.* **2003**, *150*, A149.
(25) Zhu, J.; Lu, Z.; Aruna, S. T.; Aurbach, D.; Gedanken, A. *Chem. Mater.* **2000**, *12*, 2557.